

Characterization of a microfluidic reactor for CO₂ conversion with electrolyte recycling

Citation for published version:

Lu, X, Leung, DYC, Wang, H & Xuan, J 2017, 'Characterization of a microfluidic reactor for CO₂ conversion with electrolyte recycling', *Renewable Energy*, vol. 102, no. Part A, pp. 15-20.
<https://doi.org/10.1016/j.renene.2016.10.025>

Digital Object Identifier (DOI):

[10.1016/j.renene.2016.10.025](https://doi.org/10.1016/j.renene.2016.10.025)

Link:

[Link to publication record in Heriot-Watt Research Portal](#)

Document Version:

Peer reviewed version

Published In:

Renewable Energy

General rights

Copyright for the publications made accessible via Heriot-Watt Research Portal is retained by the author(s) and / or other copyright owners and it is a condition of accessing these publications that users recognise and abide by the legal requirements associated with these rights.

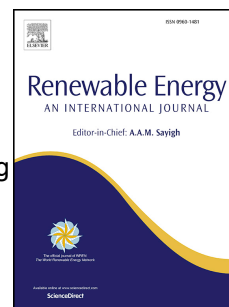
Take down policy

Heriot-Watt University has made every reasonable effort to ensure that the content in Heriot-Watt Research Portal complies with UK legislation. If you believe that the public display of this file breaches copyright please contact open.access@hw.ac.uk providing details, and we will remove access to the work immediately and investigate your claim.

Accepted Manuscript

Characterization of a microfluidic reactor for CO₂ conversion with electrolyte recycling

Xu Lu, Dennis Y.C. Leung, Huizhi Wang, Jin Xuan



PII: S0960-1481(16)30890-4

DOI: [10.1016/j.renene.2016.10.025](https://doi.org/10.1016/j.renene.2016.10.025)

Reference: RENE 8213

To appear in: *Renewable Energy*

Received Date: 13 May 2016

Revised Date: 10 October 2016

Accepted Date: 13 October 2016

Please cite this article as: Lu X, Leung DYC, Wang H, Xuan J, Characterization of a microfluidic reactor for CO₂ conversion with electrolyte recycling, *Renewable Energy* (2016), doi: 10.1016/j.renene.2016.10.025.

This is a PDF file of an unedited manuscript that has been accepted for publication. As a service to our customers we are providing this early version of the manuscript. The manuscript will undergo copyediting, typesetting, and review of the resulting proof before it is published in its final form. Please note that during the production process errors may be discovered which could affect the content, and all legal disclaimers that apply to the journal pertain.

Characterization of a Microfluidic Reactor for CO₂ Conversion with Electrolyte RecyclingXu Lu ¹, Dennis Y.C. Leung ^{1,*}, Huizhi Wang ², Jin Xuan ²¹ Department of Mechanical Engineering, The University of Hong Kong, Pokfulam, Hong Kong² Centre for Innovation in Carbon Capture and Storage (CICCS), School of Engineering and

Physical Sciences, Heriot-Watt University, Edinburgh, U.K.

* Corresponding authors, Tel.: +852 2859 7911, fax: +852 2858 5415, email: ycleung@hku.hk

(D.Y.C. Leung)

Abstract

Microfluidic fuel cells and flow batteries are free from the static physical barrier that separated the anodic and cathodic compartments, introducing the advantages of low cost and feasible miniaturized application. Recently, the concept of dual electrolyte stream proves itself an effective strategy to enhance the reactor performance by pairing catholyte and anolyte with thermodynamically favored pHs. Being able to be implemented in both fuel cell and electrolyzer modes, the dual electrolyte strategy demonstrates superior peak power density, low overpotentials, high reactivity, and high efficiency. However, keeping the characteristics of laminar flow requires continuous electrolyte flowing in the microchannel. Besides, neutralization reaction would occur within the mixing layer between the catholyte and the anolyte, requiring higher flow rate to control the layer thickness. These lead to considerable electrolyte wastage that will significantly weaken the economical aspect and electrolyte utilization efficiency. To tackle this issue, this study investigated the electrolyte degradation process and proposed an operation scheme for electrolyte recycling. Key parameters of electrolytes were tracked and monitored by mimicking different reactor situations. Results indicated that with appropriately adjusted operating conditions, electrolyte recycling would be feasible in a microfluidic pH-

differential network. Accordingly, an pH indicator for electrolyte recycling was proposed for potential practical application.

Keywords

Dual electrolyte, Electrochemistry, Microfluidics, Electrolyte recycling, pH/conductivity degradation

1. Introduction

Notwithstanding the merits of low cost, high interphasial contact area, and controlled flooding problem, low electrolyte utilization efficiency has long been a problem of flow batteries and microfluidic fuel cells. To drive the electrolyte streams and retain them within laminar characteristics, considerable amount of electrolytes is used, which, in most cases, is disposed. Many researchers have conceived the renewal or reuse of electrolytes. In the research of a quinone-bromide flow battery based on metal-free materials, Huskinson *et al.* proposed that the economical hydroxy-substituted anthraquinones could be utilized to regenerate anthraquinone-based electrolyte solutions for reuse[1]. The undesired cross contamination of anolyte and catholyte through the cell separator always occurs in a flow battery. With four different oxidation states, vanadium redox flow batteries could be used to tackle this issue as they enabled the fuel and oxidant regeneration[2]. Qiu *et al.* established a model that could help investigate and characterize the key parameters of electrolyte utilization, aiming at figuring out the electrode structures and conditions for an optimized operation[3]. However, although reducing agents could be added to recover the electrolyte, vanadium redox based flow batteries still suffered from various losses, especially electrode transport losses and electrolyte wastage. To our best knowledge, no concrete literatures could be found to firmly address this issue.

Currently, most researches on electrochemical reduction of CO₂ are based on a proton-exchange membrane, which conducts protons whilst insulates electrons and separates reactants. The high membrane cost, water management, and degradation problems, have hindered its further advancement and miniaturization. In this study, a microfluidic design was implemented, where two fluids flow co-laminarily in a micro-scale channel and perform distinctive behaviors with high surface-to-volume ratios and super-fast mass transfer rates. Microfluidics is a powerful technique to enhance the performance of reaction systems and offers a virtual but effective layer to replace conventional membrane, providing an ultimate solution towards some of the limitations of macroscale devices. The function of this virtual layer has not been fully explored until the concept of dual electrolyte was raised[4]. By coupling electrodes with corresponding thermodynamically favored pHs, not only the fuel cell performance (that is, output power density), but also the electrolysis process (that is, on-set voltage, efficiency, reactivity) could be enhanced significantly. This technique can be, and has been validated in multiple applications by many research groups[5], including the present research team[6]. Yet, the co-laminar flows of acid and alkaline would bring up an unavoidable problem, neutralization losses. The acid-alkaline neutralization reaction is a superfast reaction with a rate constant of $\sim 10^{11} \text{ M}^{-1} \text{ s}^{-1}$ and would intensify the electrolyte crossover contamination phenomenon. Therefore, identifying the degradation mechanism is the key to facilitate electrolyte recycling in the multi-dimensional electrochemistry scenario. Recently, our research group has developed a membraneless dual electrolyte reactor as a regenerative H₂/O₂ fuel cell[6] and a CO₂ conversion system[7]. By pairing electrodes with electrolytes at different pHs, the thermodynamic limitations of water window was relieved and the electrochemical performance was significantly enhanced with high output power density, round-trip efficiency and low on-set voltage. Electrode potentials were

closer to corresponding equilibrium status and hence less Joule heat loss was dissipated, facilitating the possibility of an efficient zero-carbon energy storage platform. The catholyte-anolyte interface and its associated reactant loss have also been demonstrated[8]. The impact of micro-channel thicknesses (that is, inter-electrode distances) and fluid supply rates on the fluid properties have been revealed. The electrochemical performance of the reactor dropped gradually with increasing channel thickness and the drop became significant at the channel thicknesses beyond 1000 μm . It turns out that lowering the micro-channel thickness would shorten the pathway traveled by protons, hence limiting the resistance and potential loss. The fluid supply rate has similar influence as the channel thickness. The higher the fluid supply rate is, the narrower the catholyte-anolyte interface would be. This would lead to less cross-electrolyte contamination and enhance the reactor performance. However, experimental observations suggested that when the flow rates are beyond 500 $\mu\text{L}/\text{min}$, the mixing layer perturbation could lead to instability and the excessive waste electrolytes would cause uneconomical operations.

Microfluidic electrochemistry is not only applicable for energy conversion, but also widely implemented in various fields. For instance, Fang et al. has proposed a high-sensitivity electrochemistry-based *in situ* detection methods by a microfluidic flow-through device[9]. Scialdone et al. has also achieved significant improvement of COD abatement in a microdevice[10], while Marken group has reported clean organic electrosynthetic processes based on microflow electrolysis reactions[11]. These progresses have all been benefited from the elimination of membrane constraint in a microfluidic network.

With the advantageous microfluidic technology, this study aims at improving the electrolyte utilization rate and enhancing the economical aspect by an electrolyte recycling scheme. Experimental observations and quantitative analysis implied good controllability of interface

thickness and high possibility of electrolyte reuse. With appropriate conditions, the portion of neutralized acid/alkaline, as can be quantitated and monitored by the mixing layer thickness, could be well suppressed, so does pH and conductivity as key indicators. Technically and economically, electrolyte renewal and regeneration strategy could be developed to revert the exit electrolyte streams to a qualified level for recycling operation. A prediction model was also established based on the pH degradation rate for future practical applications.

2. Methodology

2.1 Catalyst preparation

Electrodes were commercially available catalysts (Johnson Matthey) binded with carbon paper by Nafion (DuPont) solution. Pb and Pt black were used as the cathode catalyst and anode catalyst, respectively, with catalyst to Nafion ratio as 30:1. The catalyst loading was 5 mg/cm².

2.2 Cell fabrication

The electrodes were mounted at the bottom of the flow channels where co-laminar anolyte and catholyte flow. The sizes of the channels were 0.2 cm (W) × 7.5 cm (L), between which another 0.01-cm-thick PVC sheet with a 0.2 cm (W) × 0.5 cm (L) window was sandwiched to form the electrolyte contact area. The final distance between electrode surfaces was ~0.05 cm, which is an optimized value as reported in our previous parametric study[8]. A 5 cm (L) × 1 cm (W) × 0.5 cm (H) chamber was machined to be the CO₂ reservoir for the cathode side. All layered components were fabricated using a CO₂ laser ablation system (VLS 2.30, Universal Laser System) and clamped together by binder clips (Highmark).

2.3 Electrochemistry

An electrochemical station (CHI600E, CHInstruments, Inc) with a sampling frequency of 250 Hz was used to hold the cell at constant potentials. Polarization curves were obtained by

averaging the integration of a 100-second steady-state data to eliminate transient artifacts. Electrolytes were fed at a controlled flow rate, for example 500 $\mu\text{L}/\text{min}$, by syringe pumps (LSP02-1B, Longer Pump). Polarization curves of anode and cathode were recorded with digital multi-meters connected between each electrode and an external Ag/AgCl reference electrode, which was dipped in a beaker collecting the exit electrolytes. Current and power densities were normalized by the active electrode area (that is, 0.1 cm^2) and with compensated iR drop. It should be noted that unlike a typical 3-electrode system, the reference electrode for the microfluidic reactor is placed in an exit electrolyte collection beaker, which is apart from the main body. The reference electrode is linked with the working and counter electrodes by a central electrochemical station. Repetitiveness test suggested a highly repeatable experiment as has been mentioned in our previous publication[8], where the variation of measured current densities was within 10% and the range of peak Faradaic efficiencies was within 0.7%.

During the experiment of catholyte $\text{pH} = 2$ and anolyte $\text{pH} = 14$, on top of the above-mentioned experimental conditions, gaseous CO_2 ($\geq 99.5\%$ purity, Linde) was supplied at a constant flow rate of 50 sccm controlled by a mass flow controller (GFC17, Aalborg).

2.4 Formic acid determination method

To determine the concentration of the formic acid generated, the measurement method adopted a non-enzymatic allochroic reaction upon the mixture of formate and several chemicals[12]. The absorption maximum of the destination color is at 510 nm, which could be obtained by a spectrophotometer (6105 U.V./Vis. Jenway) to determine the formate concentration. 0.25 mL of collected exit electrolyte sample was extracted and diluted by 0.25 mL deionized water and 0.05 g citric acid was mixed with 1 g acetamide. Ultrasonic dispersion was then conducted in 10 mL 2-propanol, 0.5 mL of which was dissolved in a mixture of 0.5 mL of the sample, including

0.025mL 30% w/v sodium acetate and 1.75mL acetic anhydride for 1.5 hr. Before each set of experiment, standard formate solutions were prepared at concentrations of 2.5, 5, 7.5, 10, 12.5, 15, 17.5 and 20 mmol/L, whose corresponding color absorption was quantitatively determined as benchmarks by a correlative equation:

$$0.0588 \times \text{Concentration of HCOO}^- + 0.0562 = \text{Absorbance} \dots\dots\dots \text{Equ. (1)}$$

2.5 pH & conductivity measurement

The measurement of pH/conductivity was conducted by a pH/conductivity meter (Orion Star A215, Thermo Scientific). Before each set of measurements, calibration was done by dipping the pH probe into buffering solutions with pH=4.01, 7, 10.01 and conductivity probe into solutions of $12.9 \text{ mS} \cdot \text{cm}^{-1}$ and $1413 \text{ } \mu\text{S} \cdot \text{cm}^{-1}$. The pH/conductivity probe was dipped into the collected sample solutions until the readings stabilized and recorded.

2.6 Efficiency calculation

Under appropriate conditions where the electrochemical reduction reaction of CO_2 occurs, Faradaic efficiencies would be calculated to reveal the fraction of the electrons transferred for formic acid production. The measured current indicates the total electrons passing through the reaction sites and the electrons used for generating formic acid is obtained by the spectrophotometer detection. Denote the flow rate as $M \text{ L/s}$, the applied current as $N \text{ ampere}$, and HCOO^- concentration as $Y \text{ mol/L}$. The amount of electrons used for forming formic acid is $2 \times Y \times M \text{ mol/s}$. On the other hand, the total number of electrons passing through the electrode surface is $N \times K \text{ mol/s}$, where $K = 1.04 \times 10^{-5} \text{ mol/A}$ stands for the mole of electrons per ampere, concluding the equation for Faradaic efficiency as shown below:

$$\text{FE} = \frac{2 \times Y \times M}{N \times K} \times 100\% \dots\dots\dots \text{Equ. (2)}$$

3. Results and discussion

3.1 Working principle

A microfluidic reactor with electrolyte recycling was designed as shown in Figure 1. The ion concentration gradient across the microchannel, as marked and visualized by fluorescent dye, was also demonstrated. The microfluidic structure could effectively control the catholyte-anolyte interface and suppress the cross-contamination. When in need, the gaseous feed was supplied into the gas reservoir chamber on the cathode side and migrated through the gas diffusion layers (GDLs) to the catalyst surfaces. Catholyte and anolyte solutions were driven into corresponding channels by individual syringe pump, followed by collection and recirculation. As predicted, exit catholyte and anolyte were evenly distributed, validating the effective reactor design and fabrication.

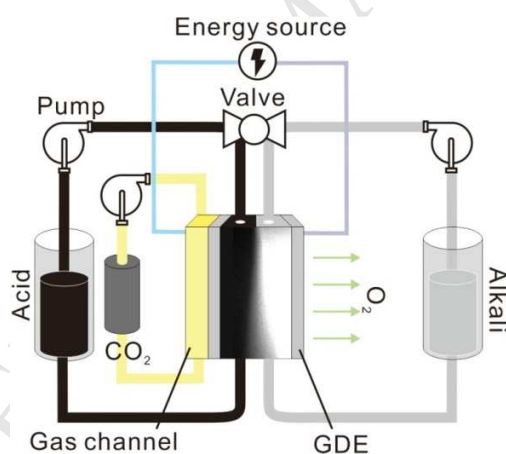


Figure 1 Schematic diagram of the microfluidic reactor with electrolyte recycling.

3.2 Benchmarks

Single electrolyte modes were regarded as benchmarks. To identify their characteristics, both single acid (catholyte pH = anolyte pH = 0) and single alkaline (catholyte pH = anolyte pH = 14) modes were established and tested as shown in Figure S1 and Figure S2, respectively.

As can be seen in Table 1, Figure S1a and Figure S2a, beyond the on-set electrolysis voltages, that is, ~2 V, the reactivity was statistically multiplied for several times in either single acid or single alkaline, and the former one increased faster. This could be explained by the fact that the acidic electrolyte conductivity was twice as much as that of its alkaline counterpart (see Table S1), enhancing the chemical kinetics.

Table 1 Comparison of reactor reactivity between single acid and single alkaline modes.

Cell voltage (V)	Current density in single acid (mA/cm ²)	Current density in single alkaline (mA/cm ²)
	Catholyte pH = Anolyte pH = 0 Electrolyte flow rate = 500 μ L/min	Catholyte pH = Anolyte pH = 14 Electrolyte flow rate = 500 μ L/min
4.0	694.2	354.8
3.7	452.3	253.3
3.4	283.4	167.1
3.1	187.8	72.2
2.8	130.0	27.7
2.5	72.4	12.1

Table S1, Figure S1d and Figure S2d suggested that during the 10-cycle operation, the electrolyte conductivity remained highly stable in single electrolyte mode, with coefficient of variation (CV) no more than 0.03. On top of the high steadiness, the small fluctuations of electrolyte conductivity were still observable, due to the balance between the ion consumption of electrochemical reactions and the productions of new species. Another key factor to evaluate the

electrolyte properties during long-term operation is the change in pH values. As shown in Table S2, Figure S1c and Figure S2c, the pH variation remained small with a CV less than 0.09, implying its high stability and low degradation rate. The low degradation of pHs and conductivity demonstrated the high feasibility of electrolyte recycling in practical applications, where not only electrolyte production and disposal costs are crucial, the number of recycling cycles is also important.

The variation of current density, however, was considerably large as can be seen from both the graphic plots (Figure S1e and Figure S2e) and the statistical results (Table 2). Comparison of CV indicated that current densities in single alkaline mode appeared relatively steady than those in single acid mode, which is due to the suppressive nature of hydroxy radical towards formate generation.

Table 2 Statistical results of current densities during the 10-cycle operation in single acid and single alkaline modes at applied potentials of 2.8, 3.4 and 4 V.

Catholyte pH = Anolyte pH = 0			
Electrolyte flow rate = 500 μ L/min			
Applied potential (V)	μ (mA/cm ²)	σ (mA/cm ²)	CV
4.0	735.3	82.5	0.11
3.4	232.5	36.6	0.16
2.8	72.9	19.3	0.26
Catholyte pH = Anolyte pH = 14			
Electrolyte flow rate = 500 μ L/min			
Applied potential	μ	σ	CV

(V)	(mA/cm ²)	(mA/cm ²)	
4.0	364.3	15.6	0.04
3.4	168.3	16.9	0.10
2.8	34.0	10.5	0.31

3.3 Effects of flow rate

With single electrolyte as the benchmark, dual electrolyte modes were tested. The catholyte and anolyte were prepared by 1 mol/L sulfuric acid and 1 mol/L potassium hydroxide, respectively. The neutralization reaction that occurred in the acid-base mixing layer brought in more complexity to the system. As shown in Figure S3a and Figure S3b, while the catholyte pHs gradually increased, cliff falls could be observed on the anolyte pHs. Afterwards, the alkaline anolyte was completely acidified. This could be explained by the fact that a sulfuric acid molecule possesses two ionizable hydrogen with a low second ionization rate[13, 14]. Upon the depletion of the first ionizable hydrogen ion, the second would be released to dominate the electrolyte solution.

Nevertheless, behind the superficial ‘cliff drop’, there actually existed a linear decrease trend in the concentration of ions (see Table 3) as could be deduced from the pH results in Table S3 by the equation $\text{pH} = -\lg[\text{H}_3\text{O}^+]$. The degradation rate dropped from 0.16 to 0.089 and then 0.06 mol/L per cycle when increasing the flow rate from 200 to 300 to 400 $\mu\text{L}/\text{min}$. The degradation rate finally stabilized at around 0.035 mol/L per cycle at flow rates of 500 $\mu\text{L}/\text{min}$ and above. In terms of number of cycles before complete acidification, it increased from 4 cycles at 200 $\mu\text{L}/\text{min}$ to 9 cycles at $\geq 500 \mu\text{L}/\text{min}$. This statistical observation implied that 500 $\mu\text{L}/\text{min}$ was the threshold of the electrolyte flow rate. At the same time, it was experimentally observed that

further increasing the flow rate would disturb the acid-alkaline interface, hence lowering the reactor performance and stability.

In Table 3, the threshold pH values, after which the anolyte pHs would drop to acid range, were extracted from Table S3 as underlined. With the CV as low as 0.005, the mean value of 13.8 could be regarded as the threshold value, upon which the electrolyte recovery should be conducted in potential practical applications.

Table 3 Statistical results of OH^- concentration degradation rate during the 10-cycle operation and threshold pH values before complete neutralization in dual electrolyte modes at flow rates from 200 to 700 $\mu\text{L}/\text{min}$. Initial catholyte $\text{pH}=0$ and anolyte $\text{pH}=14$ under zero applied voltage.

Flow rate ($\mu\text{L}/\text{min}$)	Degradation rate of OH^- concentration (mol/L per cycle)	Threshold pH before complete neutralization
200	0.160	13.71
300	0.089	13.74
400	0.060	13.74
500	0.040	13.89
600	0.037	13.85
700	0.035	13.84
		$\mu = 13.80$
		$\sigma = 0.07$
		CV = 0.005

Meanwhile, Figure S3b indicated that the electrolyte conductivity would experience a sudden change before the neutralization reaction was completed. This phenomenon was caused by two

mechanisms. Firstly, no more ions were sunk in neutralization reaction and both electrolytes were acidified. Secondly, the second ionization of sulfuric acid was massively triggered upon the threshold, supplying plenty of hydrogen ions and boosting the catholyte conductivity.

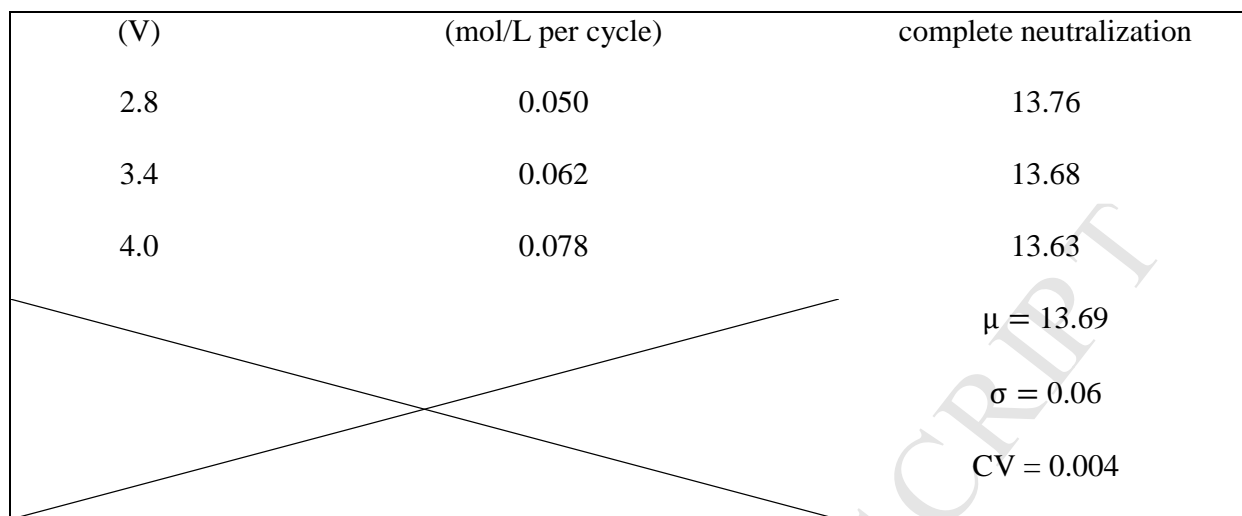
3.4 Effect of applied potential

Figure S4 demonstrated the degradation mechanism at applied potentials of 2.8, 3.4 and 4 V. The numbers of cycles which the cliff falls of pHs occurred are different for different applied potentials. The anolyte pH was acidified after 8 cycles at 4 V and 9 cycles at lower voltages. The crossover of acid-base was fiercer at elevated potentials because more ions and gaseous side products were generated, interfering the interface and accelerating the neutralization reaction. This phenomenon could be corroborated statistically. Deduced from the pHs (see Table S4), the degradation of ion concentrations (see Table 4) was observed to be linear and the degradation rate descended from 0.078 mol/L per cycle at 4 V to 0.05 mol/L per cycle at 2.8 V. The threshold pH values, as underlined in Table S4 and extracted in Table 4, were at a mean of 13.69 with a CV of 0.004.

Similar to those single electrolyte modes, sudden changes of catholyte conductivity could also be found beyond the threshold. On top of the two rationales mentioned in Section 3.3, one more ion source should not be neglected, that is, ongoing formate generation reaction at applied potentials above the on-set voltage.

Table 4 Statistical results of OH^- concentration degradation rate during the 10-cycle operation and threshold pH values before complete neutralization in dual electrolyte modes at applied potentials of 2.8, 3.4 and 4 V. Initial catholyte pH=0 and anolyte pH=14, both supplied at a flow rate of 500 $\mu\text{L}/\text{min}$.

Applied potential	Degradation rate of OH^- concentration	Threshold pH before
-------------------	---	---------------------



As shown in Figure S4c, the influence of voltages on pH variation was insignificant, but current densities were deeply affected. With the cliff falls of pHs, anolyte was acidified and the dual electrolyte mode was transformed into single acid mode. The depletion of the affiliated thermodynamic dividend of dual electrolyte mode caused sudden drops of current densities (see Figure S4e). The CV of current densities at 2.8, 3.4 and 4 V were low and close to one another (see Table 5), validating the previous finding of their corresponding threshold pHs.

Table 5 Statistical results of current densities during the 10-cycle operation at applied potentials of 2.8, 3.4 and 4 V. Initial catholyte pH=0 and anolyte pH=14, both were supplied at a flow rate of 500 $\mu\text{L}/\text{min}$.

Catholyte pH = 0 & Anolyte pH = 14			
Applied potential	μ	σ	CV
(V)	(mA/cm ²)	(mA/cm ²)	
4.0	1010.1	202.8	0.20
3.4	643.6	138.2	0.21
2.8	429.8	141.2	0.33

3.5 Effect of electrolyte ion concentration

As the thermodynamic properties of an electrochemical reactor could be adjusted by altering variables in the Nernst equation, tuning the OH^-/H^+ concentrations, that is, pHs, inevitably becomes an important strategy. In order to investigate the impact and feasibility in practical applications, three representative combinations were tested, that is, H_2SO_4 solution as catholyte and KOH solution as anolyte at the same concentrations of 1, 2, and 3 mol/L. It could be observed from Figure S5b that the limiting current density was raised from $\sim 1000 \text{ mA/cm}^2$ at 1 mol/L to $\sim 1600 \text{ mA/cm}^2$ at 3 mol/L and the reactivity was the highest at 2 mol/L (Figure S5a). The reason that 3 mol/L did not show superior reactivity was that the enhanced thermodynamic properties would promote allied side reactions and products at the same time, which were disruptive to the laminar nature of the acid-base layer.

Cliff falls of pHs appeared earlier in higher electrolyte concentration (see Figure S5c) because the neutralization reaction was much fiercer at elevated thermodynamic activity. The neutralization reaction was completed at the 6th cycle at 3 mol/L, 7th cycle at 2 mol/L and 9th cycle at 1 mol/L, followed by homogenization towards single acid mode. Higher electrolyte concentrations would quicken the ion concentration degradation and intensify the catholyte-anolyte crossover. Statistically, 1 mol/L electrolyte concentration showed significantly lower degradation rate, that is, 0.05 mol/L per cycle, compared with 2 and 3 mol/L, whose rates are 0.27 and 0.29 mol/L per cycle (see Table 6).

Different from the impact of flow rates or applied potentials, threshold pH values before complete neutralization varied with different ion concentrations, that is, 13.76 at 1 mol/L, 12.96 at 2 mol/L, and 14.18 at 3 mol/L, at a relatively high CV, that is, 0.005 (see Table 6 and S5). The reason behind was that the intrinsic nature of the electrolyte was changed and the critical points

where the OH^- would be completely depleted by H^+ were shifted as well. However, as the variation was still within the acceptable range, the mean value of the threshold pHs, that is, 13.63, was applicable as the criterion of electrolyte recovery.

Summarizing all the threshold pH values in the above-mentioned scenarios, a value of 13.7 was determined as a general threshold pH to identify the kickoff of electrolyte recovery.

Table 6 Statistical results of OH^- concentration degradation rate during the 10-cycle operation and threshold pH values before complete neutralization in dual electrolyte modes at different concentrations. Both anolyte and catholyte were supplied at a flow rate of 500 $\mu\text{L}/\text{min}$ at an applied voltage of 2.8 V.

Electrolyte pH		Degradation rate of OH^- concentration (mol/L per cycle)	Threshold pH before complete neutralization
Catholyte	Anolyte		
0.00	14.00	0.050	13.76
-0.30	14.30	0.270	12.96
-0.47	14.47	0.290	14.18
			$\mu = 13.63$
			$\sigma = 0.62$
			$\text{CV} = 0.005$

Surprisingly, the reactivity did not increase with more favorable thermodynamic settings as shown in Figure S5e and Table 7. The mean current densities and their affiliated standard deviations even dropped at high electrolyte concentrations. This was caused by the fact that more side products were generated to disturb the microfluidic characteristics as explained earlier in this section.

Table 7 Statistical results of current densities during the 10-cycle operation at different electrolyte concentrations. Both anolyte and catholyte were supplied at a flow rate of 500 $\mu\text{L}/\text{min}$ at an applied voltage of 2.8 V.

Catholyte pH	Anolyte pH	μ (mA/cm ²)	σ (mA/cm ²)	CV
0.00	14.00	429.8	141.2	0.33
-0.30	14.30	346.1	180.6	0.52
-0.47	14.47	368.7	121.0	0.33

Our previous parametric study has reported that for a CO₂ electrochemical reduction reactor, a catholyte pH = 2 and anolyte pH=14 gave the optimal performance, including reactivity and conversion efficiency[7]. The electrode potentials were closer to the equilibrium status because of the reduced electrode overpotentials. Connected to CO₂ supply, experiment was conducted on the feasibility of electrolyte recycling for this type of pH combinations, that is, unbalanced acid-base concentration.

As shown in Figure S6a and Figure S6b, with an on-set voltage reduced to ~1.8 V, the peak Faradaic and energetic efficiencies were recorded as high as 95.6% at 143 mA/cm² and 48.5% at 62 mA/cm², respectively. Although the reactor performance was raised, the pH degradation rate precluded the possibility of electrolyte recycling because the relatively weak acid catholyte was rapidly alkalinized after the first cycle as indicated by the electrolyte pHs shown in Table S6. The catholyte and anolyte pHs gradually approached each other from the 2nd cycle and are completely neutralized at the end of the 10th cycle. The whole cell was then transformed into a single alkaline mode, where the current densities and Faradaic efficiencies tended to be smooth

(see Figure S6e and Table 8). In this work, five operation scenarios, including single acid, single alkaline, dual-pH at different flow rates, dual-pH at different applied potentials and dual-pH at different ion concentrations, were tested. The electrolyte recycling scheme was successfully realized in four of them at acid-base equilibrium states, which could be used for regenerative fuel cell applications. The last scenario, that is, acid-base imbalance for CO₂ electrolysis, indicated its incompatibility with electrolyte reutilization due to the dominant ion crossover. The final formic acid concentration was recorded as 30 mmol/L, below the practical throughput requirements.

On the other hand, the trend of conductivity was smooth. Catholyte conductivity gradually increased from 82.81 to 137.5 mS/cm and that of anolyte dropped from 214.6 to 178 mS/cm. Different from other dual electrolyte modes as reported above, no sudden changes were observed because of their different dominant ion transfer mechanisms, that is, diffusion vs. neutralization. It should be noted that during the process, the CO₂ formed dissolved into the electrolytes and the generation of CO₂ conversion products would result in small fluctuations of pH and conductivity. Table 8 Statistical results of current densities during the 10-cycle operation. Initial catholyte pH = 2 and anolyte pH = 14. Both anolyte and catholyte were supplied at a flow rate of 500 μ L/min at an applied voltage of 2.8 V.

	Current density (mA/cm ²)	Faradaic efficiency (%)
μ	29.8	89.3
σ	9.8	4.9
CV	0.33	0.06

3.6 Summary and discussion

Single electrolyte mode demonstrated superior recyclability with low pH/conductivity degradation. At the same time, single acid mode illustrated higher ion transfer rate because of its higher conductivity compared with single alkaline mode. Phenomena in dual electrolyte modes, where neutralization reaction dominated, were different and the electrolyte degradation mechanism became essential. Flow rates played a major role in influencing the pH/conductivity degradation rate and the electrolyte could be recycled for 9 times at or above 500 $\mu\text{L}/\text{min}$. Another key factor was the electrolyte concentration, which could raise the neutralization rate and decrease recycling cycles. The impact of applied potentials was not significant at a voltage of 3.4 V or below, which would not quicken the electrolyte crossover. A threshold pH value of 13.7 was recommended to trigger the electrolyte recovery. It was also observed that the prerequisite of electrolyte recycling was to create an acid-base equilibrium state and the imbalance would lead to instant electrolyte cross-contamination.

4. Conclusions

Microfluidics provided a useful matrix for electrochemical devices and revealed a low cost solution towards membrane-based architecture. Exploiting the function of the virtual layer created by the microfluidic network, the pHs of electrolytes could be altered to adjust their affiliated electrode thermodynamic positions, hence improving the reactor performance. However, maintaining the laminar flow nature and controlling the virtual layer thickness required high electrolyte flow rates, leading to considerable electrolyte wastage.

This study is the first systematic investigation and demonstration of enhancing the economical aspect of a microfluidic reactor by recycling electrolytes. A deeper understanding of the reactor performance and fluid dynamic behavior was obtained, as well as the electrolyte degradation

mechanism under different operation conditions. It was observed that in a single electrolyte modes where no neutralization loss existed, electrolyte recycling was feasible and durable. In dual electrolyte modes, ion concentrations were found to degrade linearly with time and pHs would experience sudden changes. The rationale was revealed as the synergistic effects of ion sink into acid-base neutralization, ion generation from electrochemical reactions, and the second ionization of the sulfuric acid.

Higher flow rates showed positive impact on the duration of electrolyte recycling operation; yet, there existed a threshold value of 500 $\mu\text{L}/\text{min}$ and its operation duration of 27,000 seconds, beyond which the virtual layer stabilization would be disturbed. On the contrary, lower applied potentials were preferable to slow down the electrolyte cross-contamination because of the suppression of side reactions. An ion concentration degradation rate of 0.05 mol/L per cycle was observed at 2.8 V. Similar trend occurred on the initial concentrations of electrolytes. Not only the operation durations were lowered at higher electrolyte concentrations, the reactivity was also sacrificed because of the accelerated electrolyte crossover and subsequent mixing layer disruption. A threshold pH value of 13.7 was recommended as the indicator for followed-up processes, that is, electrolyte recovery. On the other hand, electrolyte recycling under the optimal pH combination for CO_2 reduction, that is, catholyte pH = 2 and anolyte pH = 14, appeared to be infeasible because of the species unbalance and consequent alkalization.

Acknowledgement

This project is financially supported by the CRCG of the University of Hong Kong and the Scottish – Hong Kong SFC/RGC Joint Research Scheme XHKU710/14 and SFC Project H15009.

References

- [1] B. Huskinson, M.P. Marshak, C. Suh, S. Er, M.R. Gerhardt, C.J. Galvin, X. Chen, A. Aspuru-Guzik, R.G. Gordon, M.J. Aziz, A metal-free organic-inorganic aqueous flow battery, *Nature* 505(7482) (2014) 195-198.
- [2] R. Ferrigno, A.D. Stroock, T.D. Clark, M. Mayer, G.M. Whitesides, Membraneless vanadium redox fuel cell using laminar flow, *Journal of the American Chemical Society* 124(44) (2002) 12930-12931.
- [3] G. Qiu, C. Dennison, K. Knehr, E. Kumbur, Y. Sun, Pore-scale analysis of effects of electrode morphology and electrolyte flow conditions on performance of vanadium redox flow batteries, *Journal of power sources* 219 (2012) 223-234.
- [4] J.L. Cohen, D.J. Volpe, D.A. Westly, A. Pechenik, H.D. Abruña, A dual electrolyte H_2/O_2 planar membraneless microchannel fuel cell system with open circuit potentials in excess of 1.4 V, *Langmuir* 21(8) (2005) 3544-3550.
- [5] S. Cheng, K.-Y. Chan, High-voltage dual electrolyte electrochemical power sources, *ECS Transactions* 25(35) (2010) 213-219.
- [6] X. Lu, J. Xuan, D.Y.C. Leung, H.Y. Zou, J.T. Li, H.L. Wang, H. and Wang, A switchable pH-differential unitized regenerative fuel cell with high power density and round-trip efficiency, *Journal of Power Sources* 314 (2016) 76-84.
- [7] X. Lu, D.Y. Leung, H. Wang, M.M. Maroto-Valer, J. Xuan, A pH-differential dual-electrolyte microfluidic electrochemical cells for CO_2 utilization, *Renewable Energy* 95 (2016) 277-285.

- 407 [8] X. Lu, D.Y. Leung, H. Wang, J. Xuan, A high performance dual electrolyte microfluidic
408 reactor for the utilization of CO₂, *Applied Energy* (2016). DOI:
409 <http://dx.doi.org/10.1016/j.apenergy.2016.05.091>
- 410 [9] T.H. Fang, N. Ramalingam, D. Xian-Dui, T.S. Ngin, Z. Xianting, A.T.L. Kuan, E.Y.P. Huat,
411 G. Hai-Qing, Real-time PCR microfluidic devices with concurrent electrochemical detection,
412 *Biosensors and Bioelectronics* 24(7) (2009) 2131-2136.
- 413 [10] O. Scialdone, A. Galia, S. Sabatino, Electro-generation of H₂O₂ and abatement of organic
414 pollutant in water by an electro-Fenton process in a microfluidic reactor, *Electrochemistry*
415 *communications* 26 (2013) 45-47.
- 416 [11] C.A. Paddon, M. Atobe, T. Fuchigami, P. He, P. Watts, S.J. Haswell, G.J. Pritchard, S.D.
417 Bull, F. Marken, Towards paired and coupled electrode reactions for clean organic microreactor
418 electrosyntheses, *Journal of Applied Electrochemistry* 36(6) (2006) 617-634.
- 419 [12] R. Sleat, R.A. Mah, Quantitative method for colorimetric determination of formate in
420 fermentation media, *Appl Environ Microbiol* 47(4) (1984) 884-885.
- 421 [13] W.L. Marshall, E.V. Jones, Second dissociation constant of sulfuric acid from 25 to 350°
422 evaluated from solubilities of calcium sulfate in sulfuric acid solutions 1, 2, *The Journal of*
423 *Physical Chemistry* 70(12) (1966) 4028-4040.
- 424 [14] A.S. Quist, W.L. Marshall, H. Jolley, Electrical conductances of aqueous solutions at high
425 temperature and pressure. II. The conductances and ionization constants of sulfuric acid - Water
426 solutions from 0 to 800° and at pressures up to 4000 Bars 1, 2, *The Journal of Physical*
427 *Chemistry* 69(8) (1965) 2726-2735.

Highlights

- Electrolyte recycling feasible on dual electrolyte microfluidic networks
- Key operation conditions optimized for better recycling operation
- pH degradation predictable for practical applications
- Reactor performance can be controlled within a stable range